An Intuitive Design Method for Disturbance-Rejecting Peak Filters

Troeng, Olof; Bernhardsson, Bo

Published in:
2018 IEEE 14th International Conference on Control and Automation (ICCA)

DOI:
10.1109/ICCA.2018.8444189

2018

Document Version:
Publisher's PDF, also known as Version of record

An Intuitive Design Method for Disturbance-Rejecting Peak Filters

Olof Troeng, Bo Bernhardsson

***Abstract*— We present a method for augmenting a nominal controller with a peak filter to achieve improved rejection of narrowband disturbances. The method is based on consideration of the open-loop Nyquist curve, which arguably makes it more intuitive and flexible than previous approaches. We also comment on some implementation aspects, and give an application example based on a control problem at a particle accelerator.**

I. Introduction

The PID controller is easy to understand and easy to tune, which makes it an attractive choice for those control applications where it gives sufficient performance. However, a common situation where the PID controller is outperformed by more advanced controllers, is when the controlled process is affected by narrowband load disturbances (e.g. from power supply switching or imbalances in a rotating system). This shortcoming of the PID controller can be understood from Francis' internal model principle [1], which states that the controller needs to contain a model of the disturbances that it hopes to reject; the PID controller is *too* simplistic in this regard.

By augmenting the PID controller (or any controller for that matter) with a second-order peak filter, it is possible to selectively increase the controller gain, and reject disturbances with a specific frequency. This approach gives only a small increase in controller complexity. The filter can be seen as a model of the narrowband disturbance; see [2] for an insightful interpretation. Peak filters have been used for improved disturbance rejection in hard-disk-drive track following [3]–[6], and several other real-world applications [7]–[9].

Although the basic idea is straightforward, there is one important detail: the phase of the peak filter needs to be carefully chosen for maintained robustness and closed-loop stability. Given its importance, it is surprising that this question has not received more attention in the literature. We are only aware of [7] and [3] that provide qualitative discussions based on root-locus arguments, and [4] that derives suitable filter coefficients by considering a transformed system.

The main contribution of this paper is a more direct and intuitive approach to designing disturbance-rejecting peak filters. The approach is based on consideration of the open-loop Nyquist curve, which makes the design trade-offs easy to understand. We will find that the most natural filter design, based on Nyquist diagram consideration, recovers the same coefficients as those in [4]. However, the flexibility of our approach makes it easy to consider other performance metrics as well. It also readily extends to complex-coefficient systems. We will also discuss the convergence time of the filter, and provide practical implementation details. Finally, as a motivating example, we consider how disturbance-rejecting peak filters can be used to improve the control performance in a particle accelerator application.

The authors are with the Department of Automatic Control, Lund University, Sweden. They work with developing the RF control system for the linear accelerator at the European Spallation Source. Email: {oloft, bob}@control.lth.se

The authors are members of the ELLIIT Excellence Center. Their work is also supported by the Swedish Research Council through the LCCC Linnaeus Center.

II. Filter Design

Given a single-input single-output plant P, and a controller C, the magnitude of the sensitivity function

$$S(i\omega) = \frac{1}{1 + P(i\omega)C(i\omega)}$$

quantifies the closed-loop robustness, and how the feedback from C affects the disturbance rejection.

We will consider how the disturbance rejection around a specific frequency ω_0 can be improved by augmenting a nominal controller (e.g., a PID controller) C_0 with a second-order filter

$$C_F(s) = \frac{s^2 + 2\zeta_z\omega_z s + \omega_z^2}{s^2 + 2\zeta_0\omega_0 s + \omega_0^2}, \tag{1}$$

where $\omega_z \approx \omega_0$, and $\zeta_z > \zeta_0$. We will refer to the filter (1) as a *peak filter* since this highlights the feature that is most relevant in this paper; the terms resonant filter and bandpass filter are also common.

If ω_z is chosen equal to ω_0, we have $C_F(0) = 1$, $C_F(\pm\infty) = 1$, and $C_F(i\omega_0) = \zeta_z/\zeta_0$, enabling the gain of the augmented controller $C = C_0C_F$ to be selectively increased at the disturbance frequency ω_0. For maintained robustness, and closed-loop stability, also the phase of the open-loop system

$$L(s) = P(s)C_0(s)C_F(s)$$

around ω_0 needs to be considered.

Choosing ω_z different from ω_0 gives two degrees of freedom—ω_z and ζ_z—making it possible to place $L(i\omega_0)$ arbitrarily in the complex plane. We will see that this allows robustness and stability to be maintained.

To clarify the behavior of the filter C_F, we introduce the parametrization

$$C_F(s) = 1 + F(s) \tag{2}$$

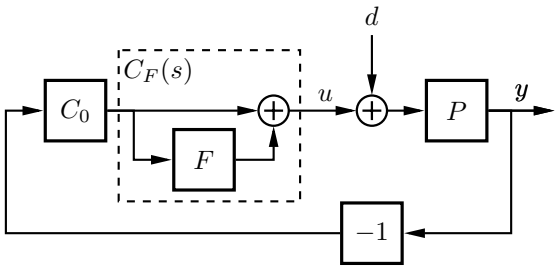

Fig. 1: By augmenting a nominal controller C_0 with a peak filter $C_F = 1 + F$ it is possible to improve the rejection of narrowband load disturbances d.

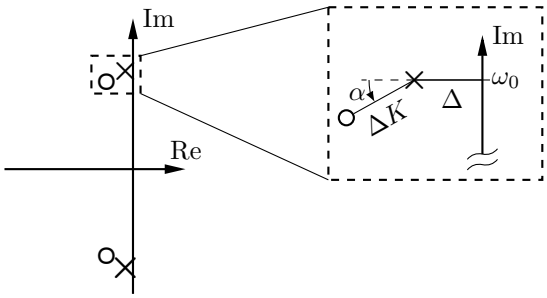

Fig. 2: Typical pole-zero diagram for the peak filter $C_F(s) = 1+F(s)$ with $F(s)$ given by (2). Having different imaginary parts for the poles and zeros gives freedom to select the phase of $C_F(s)$ at ω_0. In the limit of $\zeta_0 \to 0$, the poles are located in $p_{1,2} = -\Delta \pm i\omega_0$, and the zeros in $z_{1,2} = p_{1,2} - \Delta K e^{\pm i\alpha}$.

with

$$F(s) := K\frac{2\Delta(s\cos\alpha - \omega_0 \sin\alpha)}{s^2 + 2\Delta s + \omega_0^2}, \tag{3}$$

where K and α are new parameters, and $\Delta = \zeta_0\omega_0$. Note that $F(\pm i\omega_0) = K\mathrm{e}^{\pm i\alpha}$. The parametrization (2)–(3) is inspired by the one in [4], but we have modified it slightly to simplify the exposition[1]. See Fig. 1 for an illustration of the controller structure, and Fig. 2 for a typical pole-zero map of $C_F(s)$.

A. Nyquist Bubbles

Instead of considering the second-order filter (3) directly, we simplify the situation even further, and introduce the first-order (complex-coefficient) filter

$$B(s) = K\mathrm{e}^{i\alpha}\left(\frac{1}{2} + \frac{1}{2}\frac{1-(s-i\omega_0)/\Delta}{1+(s-i\omega_0)/\Delta}\right) \tag{4}$$
$$= K\mathrm{e}^{i\alpha}\frac{\Delta}{s - i\omega_0 + \Delta}.$$

For small ζ_0 we now have

$$F(s) \approx B(s) + B^*(s), \tag{5}$$

[1]The definition $F(s) := Ks(\omega_0\cos\alpha - s\sin\alpha)/(s^2 + 2\zeta_0\omega_0 s + \omega_0^2)$ in [4] gives that $F(i\omega_0) = K\mathrm{e}^{-\alpha}/(2\zeta_0)$, i.e., the peak amplitude depends on ζ_0, also, the minus sign in front of α makes interpretations of $F(s)$ less intuitive.

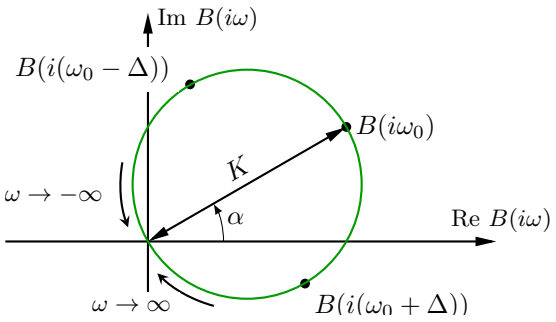

Fig. 3: The Nyquist curve of the first-order system (4).

where $B^*(s) := \overline{B(\bar{s})}$, giving that the transfer function on the right hand side has real coefficients. Equality holds in the limit[2] $\zeta_0 \to 0$.

From (4) we see that $B(s)$ is a linear fractional transformation $\mathbb{C} \to \mathbb{C}$ that maps the imaginary axis to a circle/bubble. The Nyquist curve of $B(s)$ is hence a circle with diameter K that passes through 0, and is directed at an angle α away from the origin[3]. We also see that $i\omega_0$ is mapped to the point furthest away from the origin, and that $i(\omega_0 \pm \zeta_0\omega_0)$ are mapped to points exactly in-between $B(i\omega_0)$ and the origin; see Fig. 3.

B. Nyquist Diagram Interpretation

For studying control performance and robustness, it often gives more insight to consider the Nyquist curve of the open-loop system, rather than the sensitivity function $S = 1/(1+PC)$. The distance between the Nyquist curve and the point -1 equals $1/|S(i\omega)|$, but the Nyquist curve also shows useful phase information.

To understand the effect of the peak filter, we let $L_0(s) = P(s)C_0(s)$ be the nominal open-loop system, and let $L(s) = L_0(s)C_F(s) = L_0(s)(1 + F(s))$ be the augmented system. If the peak filter is narrow, we have that

$$L(s) \approx L_0(s) + L_0(i\omega_0)F(s). \tag{6}$$

From the discussion in the previous section it is clear that the Nyquist curve of the augmented system is similar to the one of the nominal one, but with the addition of circular bubbles at frequencies $\pm\omega_0$ due to the term $L_0(i\omega_0)F(s)$. The bubble at $i\omega_0$ will be oriented in the direction $\alpha' = \alpha + \angle L_0(i\omega_0)$ and have diameter $K' = K \cdot |L_0(i\omega_0)|$; see Fig. 4 for an illustration.

[2]The exact expression is given by

$$B(s) + B^*(s) = K\frac{2\Delta\,(s\cos\alpha - \omega_0\sin\alpha + \Delta\cos\alpha)}{s^2 + 2\Delta s + \omega_0^2 + \Delta^2}.$$

[3]This is immediate from noticing that

$$B_0(s) = \frac{1}{2} + \frac{1}{2}\frac{1-s}{1+s}$$

is a linear fractional transformation that maps the imaginary axis to a circle with radius 0.5 centered around -0.5. It is also seen that $B_0(0) = 1$, $|B_0(\pm 1)| = 1/\sqrt{2}$, and $|B_0(\pm\infty)| = 0$.

C. Filter Deign for Maximum Sensitivity Reduction

For a given value of K, it is clear that maximum sensitivity reduction at ω_0 is achieved by orienting the bubbles away from the point -1. This corresponds to $\alpha' = \angle(L(i\omega_0) - (-1)$, giving

$$\begin{aligned}\alpha &= \angle\left(L_0(i\omega_0) - (-1)\right) - \angle L_0(i\omega_0) \\ &= -\angle\frac{L_0(i\omega_0)}{L_0(i\omega_0)+1} = -\angle T_0(i\omega), \quad (7)\end{aligned}$$

where $T_0 = L_0/(1+L_0)$ is the complementary sensitivity function of the nominal system.

The choice (7) is the same as in [4]. However, the line of argument that we used to arrive at this, arguably provides more intuition.

Choosing α according to (7) and

$$K = \frac{N}{|S_0(i\omega_0)|}\frac{1}{|L_0(i\omega_0)|} = \frac{N}{|T_0(i\omega_0)|}, \quad (8)$$

we get a sensitivity reduction at ω_0 by a factor $(N+1)$. The choices (7) and (8) are illustrated in Fig. 4.

D. Closed-Loop Behavior

With the choices of α and N in (7)–(8), we can derive an approximate expression for how the filter affects the closed-loop sensitivity around ω_0. First, re-write the sensitivity function of the augmented system as

$$\begin{aligned}S(s) &= \frac{1}{1+L_0(s)(1+F(s))} \\ &= \underbrace{\frac{1}{1+L_0(s)}}_{S_0(s)}\cdot\frac{1}{1+T_0(s)F(s)}. \quad (9)\end{aligned}$$

Then, using (7), (8), and that $T_0(s)F(s) \approx T_0(i\omega_0)F(s)$,

$$S(s) \approx S_0(s)\frac{s^2+2\zeta_0\omega_0 s+\omega_0^2}{s^2+2(N+1)\zeta_0\omega_0 s+\omega_0^2}. \quad (10)$$

For $N > 0$ the second factor (10) is a notch filter, with a convergence time on the order of $\tau_F = 1/((N+1)\omega_0\zeta_0)$. Thus, the time it takes for the peak filter to reject a narrowband disturbance is given by τ_F.

Since $(N+1)\omega_0\zeta_0$ is the 3 dB bandwidth of the notch around ω_0, the same number also determines the degradation of the closed loop at frequencies away from ω_0, due to the waterbed effect. In [4] a similar discussion, but only the behavior *at* the frequency ω_0 was considered.

E. Implementation Aspects

When the filter C_F is used for augmenting a PI(D) controller, it will probably be advantageous to place it before the PI(D) controller in order to reduce the impact on the anti-windup implementation. Perhaps, it is even better to place the filter as in Fig. 5, since there is no need to filter the reference signal through the peak filter.

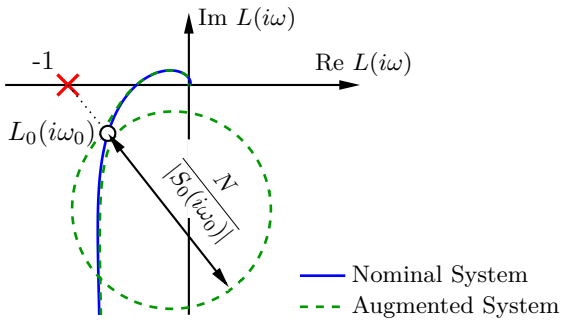

Fig. 4: By augmenting a nominal controller with a peak filter, it is possible to introduce a bubble in the open-loop Nyquist curve, moving the Nyquist curve at ω_0 to an arbitrary point. The figure illustrates when the filter parameters are chosen according to (7) and (8), which gives a sensitivity reduction at ω_0 by a factor $(N+1)$.

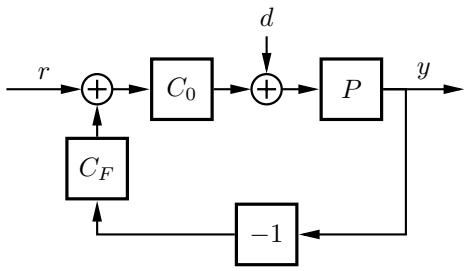

Fig. 5: For a practical implementation it could be beneficial to avoid filtering the reference signal through the peak filter, as is shown in this figure.

A discrete time counterpart to the filter (1) obtained through pole-zero matching is given by

$$\begin{aligned}C_F(z) &= \frac{(z-r_z e^{i\omega_z h})(z-ze^{-i\omega_z h})}{(z-r_0 e^{i\omega_0 h})(z-r_0 e^{-i\omega_0 h})} \\ &= \frac{z^2-2r_z\cos(\omega_z h)z+r_z^2}{z^2-2r_0\cos(\omega_0 h)z+r_0^2},\end{aligned}$$

where h is sample time, $r_0 = e^{-\zeta_0\omega_0 h}$ and $r_z = e^{-\zeta_z\omega_z h}$.

F. Design Guidelines

The filter $F(s)$ in (3) has four parameters, which gives us four degrees-of-freedom that allow us to select

- The peak frequency
- The peak phase
- The magnitude of the peak
- The width of the peak (i.e., settling time, robustness, numerical stability)

A typical approach to select the parameters in the peak filter (3) would be:

1) Select ω_0 as the disturbance frequency.
2) Select the desired sensitivity reduction N at ω_0, and put $K = N/|T_0(i\omega_0)|$.
3) Select Δ (ζ_0) based on consideration of the spectral width of the disturbance, the required convergence time, and numerical implementation considerations.

4) Select α to achieve the best possible robustness, the typical choice would be according to (7).

Some comments on point 3) are in order. If it is considered more important to maintain a large amplitude or phase margin, it would make sense to choose α different from (8). Another case where a different value of α should be considered, is when the bubbles are far away from their ideal circular shape. This is seen in Figure 11a, where a small increase of α would improve the closed-loop robustness. Note that the intuition provided in this section makes these modifications obvious.

G. Remarks

Remark 1: In the case of complex-coefficient systems [10], the frequency response and disturbance spectrum might not be symmetric about the zero frequency. This case is easy to handle by working directly with the Nyquist bubbles (4). For example, if L_0 is not conjugate symmetric, the two bubbles at $\pm\omega_0$ should have their parameters chosen differently. If the disturbance only occurs at one side of the frequency spectrum, one may use a single bubble.

Remark 2: From expression (1) it is clear that the maximum of $|C_F(i\omega)|$ might not occur at ω_0. For example, with $\omega_0 = 10$, $\omega_z = 2$, $\zeta_0 = 0.1$ and $\zeta_z = 0.2$. the maximum is achieved at $\omega^\star = 9.77$. However, if the maximum gain ζ_z/ζ_p of (1) is large, then the distance between ω_0 and the peak frequency $\omega^\star$ will be small.

III. Particle Accelerator Application

As an application example, we design peak filters for reducing the regulation errors of the accelerating electromagnetic fields in the linear particle accelerator at the European Spallation Source[4]. The accelerating fields will be confined in 155 radio-frequency (RF) cavities, each driven by a dedicated RF amplifier, see Fig. 6. The RF amplifiers will be controlled by feedback loops that keep the amplitudes and phases of the accelerating fields constant, which is crucial to accelerator operation.

The accelerator will be pulsed at 14 Hz, with a peak power consumption of about 200 MW. To meet the grid-flicker requirements of regional power grid, many of the DC power supplies for RF amplifiers have been designed in-house. Simulation results[5] indicate that the output voltage of the DC supplies will contain a narrowband disturbance at 90 kHz, see figures 7 and 8. The ripple will couple to the output of the RF amplifiers, acting as a disturbance on the cavity fields.

The discussed peak filters provide a convenient tool to reduce the impact of this disturbance. Given the large number of plants with varying dynamics, it becomes important with a straight-forward and intuitive design method, such as the one discussed previous section.

[4]A neutron spallation facility that is currently under construction outside of Lund, Sweden [11]

[5]Provided by the Power Converter group at ESS in Nov. 2015.

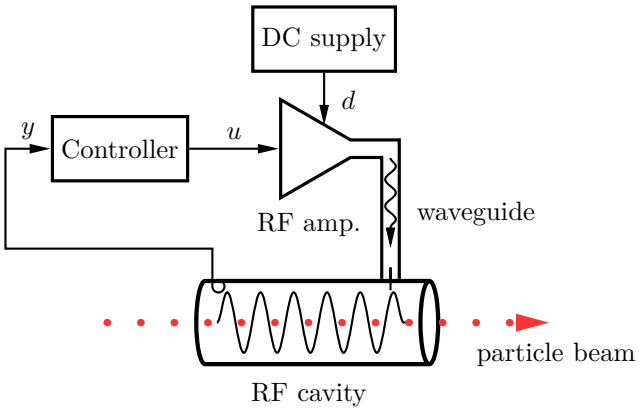

Fig. 6: Illustration of an RF station, and the feedback loop that controls the amplitude and phase of the accelerating electromagnetic field in the cavity.

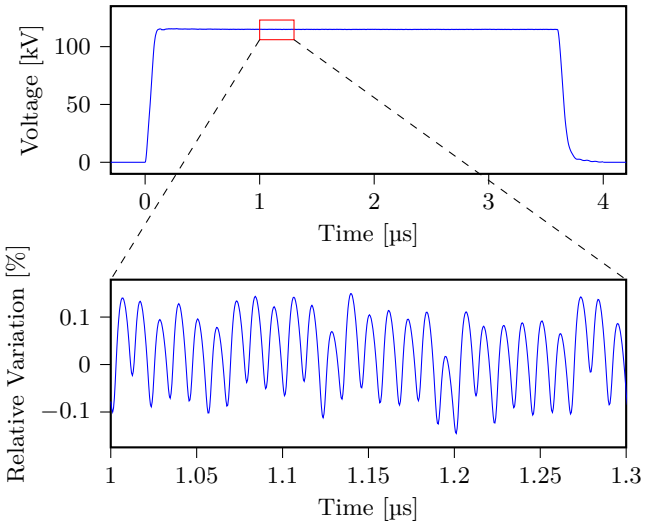

Fig. 7: Voltage pulse of the DC power supply. The zoom reveals the presence 90 kHz switching ripple.

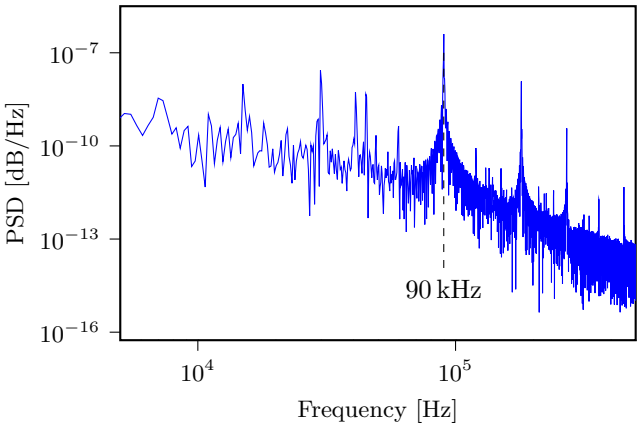

Fig. 8: Power spectral density of the DC supply ripple. The dominant harmonic at 90 kHz lies in the frequency range where the disturbance rejection of the cavity feedback loop is the worst.

A. Process Description

To keep the exposition simple, we only consider the phase dynamics of the cavity control loop. A normalized baseband model is given by

1) Plant Dynamics:

$$P(s) = \frac{\gamma}{s+\gamma} \mathrm{e}^{-s\tau}, \tag{11}$$

where γ is the cavity bandwidth, and $\tau = 1\,\mu\mathrm{s}$ is the loop delay (from signal processing in the controller and electromagnetic wave propagation in the waveguide and the measurement cable). We have neglected amplifier dynamics, nonlinearities, parasitic cavity modes, and detuning; see [10] for a more detailed model.

In our numerical example we will consider three cavity types with different bandwidths γ,

- Radio-Frequency Quadrupole (RFQ), $\gamma/(2\pi) = 55\,\mathrm{kHz}$
- Drift-Tube Linac (DTL), $\gamma/(2\pi) = 12\,\mathrm{kHz}$
- Elliptical medium-β cavity, $\gamma/(2\pi) = 0.5\,\mathrm{kHz}$.

2) Impact of DC Supply Ripple: The supply ripple acts on the cavity field as an input load disturbance given by

$$d(t) = K_g \xi \Delta_{\mathrm{supp}}(t),$$

where $\Delta_{\mathrm{supp}}(t)$ is the relative voltage variation of the DC supply, the factor K_g relates relative variations of the RF drive to relative variations on the cavity field [10], and ξ is the phase-pushing factor of the RF amplifier[6]. Typically $1 \le K_g \le 2$, and the RF amplifiers that will drive the considered cavities have $\xi \approx 10°/\%$.

3) Nominal Controller Design: Given the simple plant dynamics (11), the PI(D) is an appropriate choice for suppressing low-frequency disturbances. For each cavity type, a nominal PID controller C_0 was designed for rejection of low-frequency disturbances, subject to constraints on the control signal activity and $||S_0(i\omega)||_\infty \le 1.6$.

A typical transfer function from load disturbances d to control errors, when the cavity is controlled by a PID controller is shown in Fig. 9. It is seen that the disturbance rejection is worst at around 50 kHz–100 kHz, which is due to the fundamental limitations from the 1 µs loop delay.

B. Peak Filter Design

The nominal controllers were augmented with peak filters designed according to (7) and (8). The same peak filter parameters were used for all three cavity types: $\omega_0 = 90\,\mathrm{kHz}$, $\zeta_0 = 0.015$, and $N = 6$.

C. Simulation Results

The improvement from the peak filters in terms of rejecting the ripple in Fig. 8 is shown in Table I. The Nyquist plots for the different designs are shown in Fig. 11. Note that the bulges from the peak filters are oriented quite different, showing the advantage with an automatic design procedure.

[6]Variations of the DC supply voltage also affects the amplitude of the output, but to a much smaller extent [12].

TABLE I: Control performance for PID controllers with and without peak filters. The numbers *only* include the impact of DC supply ripple—during operation there will be many additional disturbances.

	RFQ	**DTL**	**Medium-β**
Bandwidth $\gamma/(2\pi)$ [kHz]	55	12	0.5
K_g	1.3	1.3	2
Phase error (rms)			
Requirement	0.20°	0.20°	0.10°
PID	0.51°	0.16°	0.013°
PID + peak filter	0.13°	0.05°	0.008°

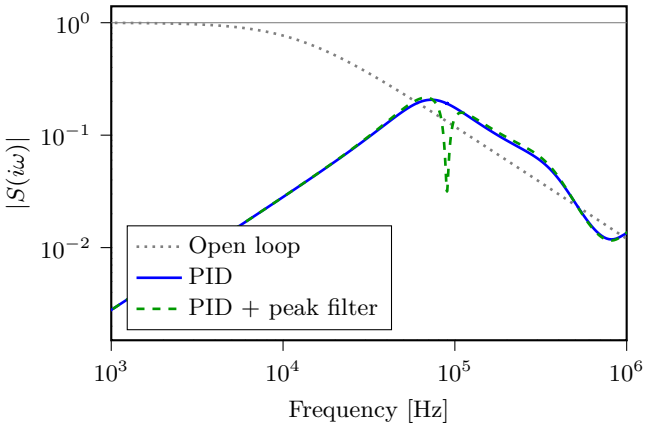

Fig. 9: Transfer functions from load disturbances d to cavity field errors for a DTL, with different controllers.

The transfer function from disturbances to control errors for a DTL and different controllers are shown in Fig. 9, and the corresponding power spectra are shown in Fig. 10. As can be seen in Fig. 9, there is significant improvement in rejection of the disturbance at 90 kHz, with small performance degradation for other frequencies. The Nyquist plots in Fig. 11 show that the the filters only give a small impact on robustness.

D. Discussion

The presented approach, where a peak filter is introduced to selectively increase the controller gain at a specific frequency, allows the rejection of narrowband disturbances at a low *implementation* cost. However the approach relies on that the center frequency of the narrowband disturbance is known, and it gives a more complex controller with four additional parameters that need to be correctly tuned.

IV. Summary

We have provided an interpretation in the open-loop Nyquist diagram for how to selectively increase the controller gain at a specific frequency without significantly degrading the closed-loop robustness; this provides a better understanding of how to do loop shaping for rejection of narrowband disturbances.

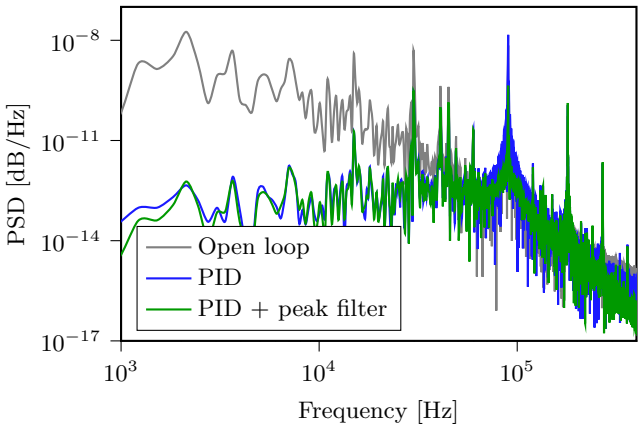

Fig. 10: Power spectral density of the cavity field error for a DTL with the DC supply ripple in Fig. 8, and the three controllers in Fig. 9. It is seen that the ripple filter significantly reduces the impact of 90 kHz ripple.

We have also discussed a motivating example of how narrowband disturbance rejection could improve the control performance in a particle-accelerator application.

References

[1] B. A. Francis and W. M. Wonham, "The internal model principle of control theory," *Automatica*, vol. 12, no. 5, pp. 457–465, 1976.

[2] K. J. Åström and T. Hägglund, *Advanced PID Control*. Research Triangle Park, NC: The Instrumentation, Systems, and Automation Society, 2006.

[3] Y. Kim, C. Kang, and M. Tomizuka, "Adaptive and optimal rejection of non-repeatable disturbance in hard disk drives," in *Proc. IEEE/ASME Int. Conf. Adv. Intelligent Mechatronics*, vol. 1, 2005, pp. 1–6.

[4] J. Zheng, C. Du, G. Guo, *et al.*, "Phase lead peak filter method to high TPI servo track writer with microactuators," in *Proc. Am. Control Conf.*, IEEE, 2006, pp. 1309–1314.

[5] T. Atsumi, A. Okuyama, and M. Kobayashi, "Track-following control using resonant filter in hard disk drives," *IEEE/ASME Trans. Mechatronics*, vol. 12, no. 4, pp. 472–479, Aug. 2007.

[6] J. X. Xu, D. Huang, V. Venkataramanan, *et al.*, "Adaptive compensation of contact-induced vibration in high density hdd servo systems using peak filter method," in *IEEE Int. Symp. on Ind. Electronics*, May 2012, pp. 797–802.

[7] L. A. Sievers and A. H. von Flotow, "Comparison and extensions of control methods for narrow-band disturbance rejection," *IEEE Trans. Signal Process.*, vol. 40, no. 10, pp. 2377–2391, 1992.

[8] C.-H. Han, C.-C. Wang, and M. Tomizuka, "Suppression of vibration due to transmission error of harmonic drives using peak filter with acceleration feedback," in *Proc. 10th IEEE Int. Workshop on Adv. Motion Control, 2008.*, 2008, pp. 182–187.

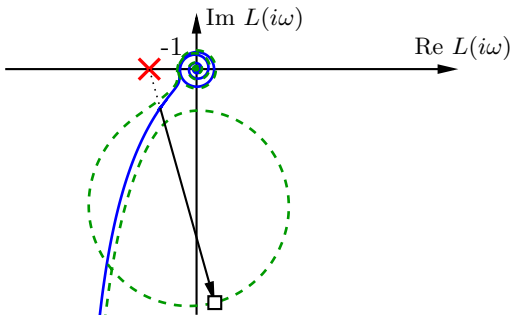

(a) Radio-frequency quadrupole.

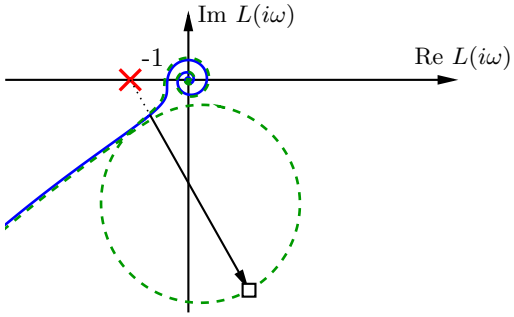

(b) Drift-tube linac.

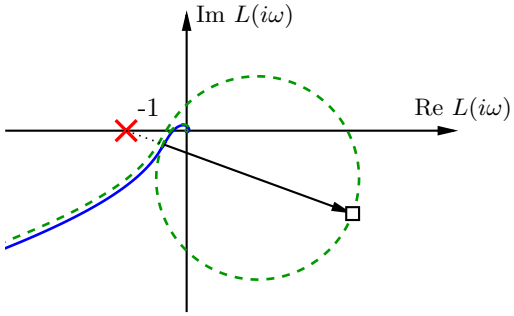

(c) Elliptical medium-β cavity.

Fig. 11: Nyquist curves for three different field control loops. The blue solid lines correspond to nominal open-loop systems, and the green dashed lines to systems augmented with peak filters.

[9] M. Castilla, J. Miret, J. Matas, *et al.*, "Control design guidelines for single-phase grid-connected photovoltaic inverters with damped resonant harmonic compensators," *IEEE Trans. Ind. Electron*, vol. 56, no. 11, pp. 4492–4501, Nov. 2009.

[10] O. Troeng, "Cavity field control for high-intensity linear proton accelerators," Licentiate thesis, Lund University, Sweden, 2017.

[11] S. Peggs, R. Kreier, C. Carlile, *et al.*, "ESS technical design report," European Spallation Source, Tech. Rep. ESS-doc-274, 2013.

[12] R. Zeng, A. Johansson, K. Rathsman, *et al.*, "Influence droop and ripple of modulator on klystron output," European Spallation Source, Tech. Rep. ESS-AD-0033, 2011.